Validation of MRI- and CT-based Finite Element Modeling of the Proximal Femur Under Sideways Fall

Benjamin D. Olowu[1], Joshua D. Auger[1], Elise F. Morgan[1,2]
[1]Department of Mechanical Engineering, [2]Department of Biomedical Engineering, Boston University, Boston, MA,USA
benolowu@bu.edu

Disclosures: Benjamin D. Olowu (N) Joshua D. Auger (N), Elise F. Morgan (N)

INTRODUCTION: Fractures of the hip represent ~20% of all fragility fractures [1], and falls to the side of the hip cause over 90% of hip fractures [2]. These injuries are associated with substantial morbidity, mortality, and healthcare costs, making accurate prediction of bone strength and fracture risk a critical priority. While computed tomography (CT) is the current standard for image-based, patient-specific finite element (FE) simulations of hip fracture [3,4], the relatively high dose of radiation with CT [3, 5] makes magnetic resonance imaging (MRI)-based FE modeling an attractive alternative [6]. However, validation of MRI-based FE models is still ongoing. Prior MRI-based modeling used T2-weighted MRI and found good agreement with mechanical testing [6,7]. Other sequences, such as proton density (PD)-weighted spin-echo, also used in bone assessment [8-10], have not yet been evaluated. Thus, the goal of this study was to evaluate the predictive capacity of PD-weighted MRI-based models by comparing them with paired CT-based FE models and experimental data.

METHODS: Fresh-frozen human cadaveric femora (n=10, 6M/4F, age range = 25–84 years) underwent CT (voxel size = 0.625 x 0.625 x 0.625 mm; GE HealthCare Technologies) and MRI scans (voxel size = 0.332 x 0.332 x 0.332 mm; proton density-weighted spin-echo sequence, TR/TE = 4712/28.176 ms; 3-T GE Discovery 750W scanner). From the images, the proximal femur was semi-automatically segmented and converted to a second-order tetrahedral mesh (MITK-GEM, SimTK). MRI-based material mapping followed published methods [7,11], where bone volume fraction (BV/TV) was approximated by an inverted linear scaling that assigned the upper and lower 2.5% of MRI gray values to pure marrow (0% BV/TV) and pure bone (100% BV/TV), respectively. Element-wise elastic modulus for MRI models was assigned as linearly proportional to mean BV/TV value [6]. CT scans used a calibration phantom to obtain CT density, which was then converted to apparent density [12] and mapped to modulus using an established density–modulus relation [13]. To isolate the influence of the different image segmentations for MRI vs CT, we ran a separate set of simulations using a homogenous Young's modulus (10GPa) throughout. Poisson's ratio was 0.3 for all models. Sideways fall boundary conditions (10° adduction, 15° internal rotation) were prescribed [14] with a hinge constraint at the distal end, a roller constraint at the greater trochanter, and a compressive load of 2000 N applied to the femoral head (Fig. 1a). Each femur was then tested experimentally in a sideways fall configuration (Fig. 1b). One specimen was excluded from analysis due to machine malfunction. Whole bone stiffness, and femoral strength were computed, the latter via an asymmetric maximum principal strain criterion (0.73% tension, 1.04% compression) to predict failure load and location [15]. Linear regression and paired t-tests were used to compare MRI and CT predictions to experimental outcomes and to each other.

RESULTS: MRI-based models showed poor agreement with experimental outcomes. No correlation was found for either whole bone stiffness ($R^2 = 0.07$, $p=0.29$) or failure load (Fig. 2a; $R^2 = 0.16$, $p=0.50$). In contrast, for the CT-based models, whole bone stiffness ($R^2 = 0.56$, $p=0.020$) and failure load ($R^2 = 0.60$, $p=0.014$) correlated well with experiment. Relative to experiment, MRI-based models overpredicted stiffness by 317% and failure load by 89% whereas CT-based models overpredicted stiffness by 144% but slightly underpredicted failure load by only 11.5%. Compared with CT, MRI-based models were slightly smaller in volume (−9.8%, $p<0.001$) but had 266% higher median elastic modulus ($p<0.001$), 72% higher predicted stiffness ($p<0.001$), and 136% higher failure load ($p=0.032$; Fig 2b, left). However, in the homogenous-material case, MRI-derived predictions of stiffness and failure load were no different from their CT counterparts (Fig 2b, right).

DISCUSSION: This is the first study to directly compare PD-weighted MRI FE modeling with standard CT-based modeling of the proximal femur under sideways fall. Whereas the CT-based models showed good correlation with experimental measurements of stiffness and failure load, the MRI-based models correlated poorly. Stiffness was overestimated by both the models from both imaging modalities, while failure load was slightly underpredicted by CT models, but overpredicted by MRI models. Predicted metrics did not differ between CT- and MRI-based models when both models were assigned homogeneous material properties, indicating that PD-weighted MRI images enable sufficient accuracy in segmentation of the proximal femur. However, the substantial differences in stiffness and failure load between CT- and MRI-based models in the case of heterogeneous material mapping suggests that the relationship previously formulated for T2-weighted MRI does not directly translate to PD-weighted MRI. That prior formulation led to overestimation of elastic modulus in MRI-based models (Fig. 3). Future work exploring relationships between PD-weighted MRI signal values and measures of density or modulus would advance MRI-based FE framework as a fracture risk assessment tool.

SIGNIFICANCE/CLINICAL RELEVANCE: Although MRI-based models may offer a radiation-free alternative to CT-based FE modeling, the ability of PD-weighted MRI-based FE models to predict the mechanical response of the proximal femur is contingent on an improved relationship between PD-weighted MRI signal and tissue material properties.

REFERENCES: [1] Johnell et al., *Osteoporos. Int*., 2006; [2] Parkkari et al., *Calcif. Tissue Int.*, 1999; [3] Adams et al., *JBMR,* 2018; [4] Fleps et al., *Bone,* 2022; [5] Kopperdahl et al., *JBMR,* 2014 [6] Rajapakse et al., *Bone,* 2020; [7] Rajapakse et al., *Curr. Osteoporos. Rep*., 2018; [8] Wehrli et al., *JMRI,* 2007; [9] Jerban et al., *Fendo*., 2020 [10] Majumdar et al., *TMRI,* 2002; [11] Chang et al., *MAGMA*, 2015; [12] Schileo et al., *J. Biomech*, 2008, [13] Morgan et al., *J. Biomech*, 2003; [14] Dragomir-Daescu et al., *Ann. Biomed. Eng.,* 2011; [15] Schileo et al., *J. Biomech*, 2014; [16] Helgason et al., *Med. Eng. Phys.,* 2016

ACKNOWLEDGEMENTS: NIH AR071657; NIH AG073671

IMAGES AND TABLES:

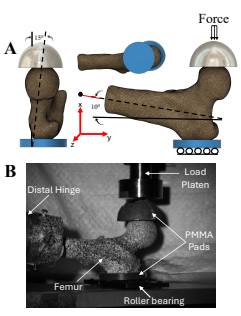

Fig. 1: Sideways fall configuration. (A) FE boundary condition and (B) Experimental setup

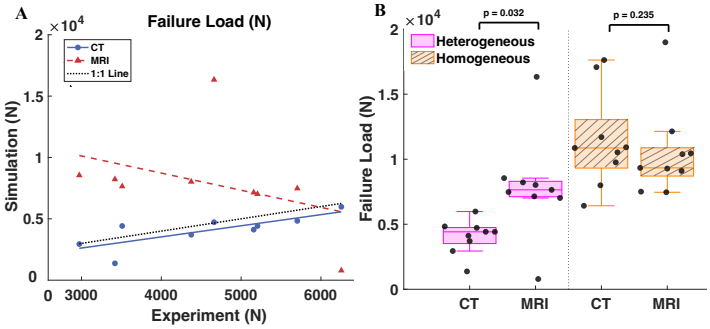

Fig. 2: (A) Failure load comparison between simulation and experiment, (B) MRI- and CT- predicted failure load with heterogeneous and homogeneous material mapping

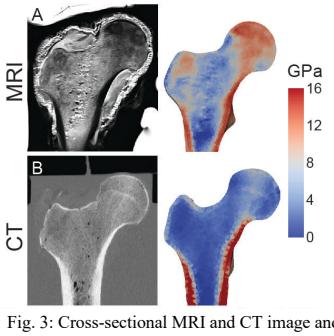

Fig. 3: Cross-sectional MRI and CT image and corresponding modulus distribution for a representative specimen.